Correlating Structural Dynamics and Function in Single Ribozyme Molecules

Xiaowei Zhuang,[1]* Harold Kim,[1] Miguel J. B. Pereira,[2] Hazen P. Babcock,[1]* Nils G. Walter,[2]† Steven Chu[1]†

We have studied the correlation between structural dynamics and function of the hairpin ribozyme. The enzyme-substrate complex exists in either docked (active) or undocked (inactive) conformations. Using single-molecule fluorescence methods, we found complex structural dynamics with four docked states of distinct stabilities and a strong memory effect where each molecule rarely switches between different docked states. We also found substrate cleavage to be rate-limited by a combination of conformational transitions and reversible chemistry equilibrium. The complex structural dynamics quantitatively explain the heterogeneous cleavage kinetics common to many catalytic RNAs. The intimate coupling of structural dynamics and function is likely a general phenomenon for RNA.

RNA plays a central role in cellular processes such as splicing and translation (*1*). In addition to a number of protein-independent RNA enzymes (ribozymes), recent insights into the structure and function of large ribonucleoproteins suggest that ribosomes, and perhaps spliceosomes, are also "ribozymes" in which the RNA constituents play the major catalytic role (*2–5*). The catalytic activities of ribozymes depend critically on their folded structures, and the complex structural dynamics of RNA may impose consequences on their catalytic functions, a relationship that is still poorly understood.

Small ribozymes provide critical model systems for structural dynamics–function studies (*6*), but despite their apparent simplicity, little is known about the structural dynamics of these enzymes. Here, we used fluorescence resonance energy transfer (FRET) to study the structural dynamics of the hairpin ribozyme at the single-molecule level (*7–10*). Our results show that the structural dynamics of RNA can be very complex and is intimately coupled to its function.

The hairpin ribozyme is derived from the autocatalytic negative strand of the tobacco ringspot virus satellite RNA (*11*). The minimal active form of the ribozyme of ~50 nucleotides consists of the two independently folding helix-loop-helix domains A and B (Fig. 1A). This RNA can form an extended conformation with the two domains coaxially stacked (undocked state), or it can form a bent conformation with tertiary interactions between loops A and B (docked state) (*12, 13*). The structures of the isolated domains and that of the docked ribozyme have been studied by biochemical methods (*14, 15*), nuclear magnetic resonance (NMR) (*16, 17*), and x-ray crystallography (*18*).

The hairpin ribozyme reversibly cleaves its substrate (S) into two products (3′P and 5′P). Previous studies (*12*) have suggested a multistep reaction pathway (Fig. 1B): (i) Substrate S binds to the ribozyme, resulting in the undocked conformation; (ii) the complex folds into the docked state; (iii) cleavage occurs; and (iv) the complex undocks and the cleavage products dissociate, or vice versa. In this work, the proposed reaction pathway has been largely verified and many of the kinetic rate constants have been measured. With these rate constants, the rate-limiting steps of the overall cleavage reaction (*19*, *20*) have been determined and the heterogeneity in cleavage reaction kinetics (*21, 22*) can now be understood.

Figure 1A shows the ribozyme construct used in our experiments (*23*). The dye molecules Cy3 (donor) and Cy5 (acceptor) are attached to the 3′ and 5′ ends of the RzA strand, respectively, and serve as the FRET pair. Biotin attached to the 5′ end of strand RzB allows the molecule to be immobilized on a surface via the streptavidin-biotin interaction (*7*). The donor and acceptor fluorescence of single ribozyme molecules was detected using a total internal reflection or scanning confocal microscope (*7*).

First, we measured the cleavage activity of the surface-immobilized ribozyme by monitoring FRET between Cy3 and Cy5. The FRET value is defined as $I_A/(I_A + I_D)$, where I_D and I_A are the fluorescence intensities of the donor and acceptor, respectively. Low

[1]Department of Physics, Stanford University, Stanford, CA 94305, USA. [2]Department of Chemistry, University of Michigan, Ann Arbor, MI 48109, USA.

*Present address: Department of Chemistry and Chemical Biology, Harvard University, Cambridge, MA 02138, USA.
†To whom correspondence should be addressed. E-mail: nwalter@umich.edu, schu@stanford.edu

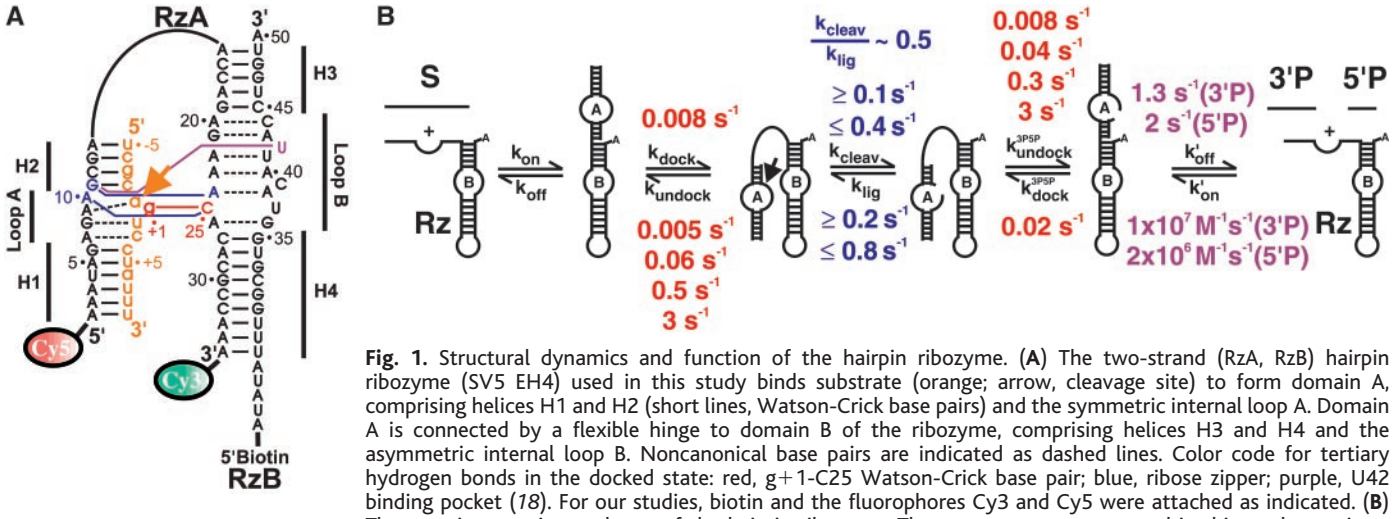

Fig. 1. Structural dynamics and function of the hairpin ribozyme. (**A**) The two-strand (RzA, RzB) hairpin ribozyme (SV5 EH4) used in this study binds substrate (orange; arrow, cleavage site) to form domain A, comprising helices H1 and H2 (short lines, Watson-Crick base pairs) and the symmetric internal loop A. Domain A is connected by a flexible hinge to domain B of the ribozyme, comprising helices H3 and H4 and the asymmetric internal loop B. Noncanonical base pairs are indicated as dashed lines. Color code for tertiary hydrogen bonds in the docked state: red, g+1-C25 Watson-Crick base pair; blue, ribose zipper; purple, U42 binding pocket (*18*). For our studies, biotin and the fluorophores Cy3 and Cy5 were attached as indicated. (**B**) The putative reaction pathway of the hairpin ribozyme. The rate constants measured in this work are given. [Details of the experiments determining these rate constants are described in the text and (*25*).]

FRET occurs when the enzyme is in the undocked state, with the distance between the 3′ and 5′ ends of the RzA strand estimated to be ~8 nm (*24*). High FRET occurs in the docked state (~3 nm), and intermediate FRET is seen when S is not bound (~6 nm) (*24*). A FRET distribution of ribozyme molecules during the cleavage reaction is shown in Fig. 2. The population of S-free ribozyme grows with time as a result of cleavage and product release. The reaction time course shows heterogeneous reaction kinetics with two distinct cleavage rate constants. Identical reaction kinetics were found free in solution for the same ribozyme construct (Fig. 2) and for the unlabeled ribozyme (*21*). Thus, the functional properties of the hairpin ribozyme are not compromised by surface immobilization and dye labeling.

Next, we studied the conformational changes of the ribozyme upon S binding. After S binding, 98 to 99% of the single-molecule FRET time trajectories (Fig. 3A) show a FRET decrease; this finding indicates that the molecule enters the undocked state before attaining the catalytically active docked conformation. Then the molecule switches stochastically between the undocked and docked states.

We found direct evidence that cleavage occurs only in the docked state, as previously suggested (*12*). Figure 3B shows a typical FRET time trace of cleavable substrate S bound to a single ribozyme. The final FRET jump to an intermediate level signals the release of cleavage products. Among the several hundred traces examined, 90 to 95% show transitions to the S-free state from the docked state. The fraction (5 to 10%) showing the transition from the low-FRET state is consistent with the contributions from short docked events (which were missed because of our 2-s time resolution) and from slow substrate dissociation (*11*). Thus, cleavage only occurs in the docked state.

The docking and undocking kinetics can be deduced from the dwell times of the molecules in the undocked and docked states, respectively (Fig. 3A) (*7*). The dwell times in the undocked state can be described by a single rate constant for docking, $k_{dock} = 0.008\ s^{-1}$. The dwell times in the docked state show a complex behavior, with at least four rate constants for undocking: $k_{undock,1} = 0.005\ s^{-1}$, $k_{undock,2} = 0.06\ s^{-1}$, $k_{undock,3} = 0.5\ s^{-1}$, and $k_{undock,4} = 3\ s^{-1}$ (Fig. 4) (*25*). Fewer rate constants or a Gaussian distribution of rate constants do not sufficiently describe the data. This finding suggests the existence of four distinct docked states. The docking and slowest undocking rate constants compare well with previously estimated rate constants for docking and undocking from ensemble solution measurements (*12*). The three less stably docked states were not detected previously. Their fast undocking means that these states are not significantly populated at any time, making them practically impossible to detect by ensemble methods.

The time trajectories of individual molecules reveal a pronounced "memory" effect (*26–29*). Individual molecules tend to repeat similar dwell times in the docked state, which suggests that certain structural features in the docked states are "remembered" by the molecule after undocking (Fig. 5A) (*25*). Preliminary results show slow switching between different undocking kinetics (Fig. 5B). At most 5% of the trajectories show such switching in 3 hours, indicating slow dynamics of the structural features that determine the undocking kinetics.

What is the mechanism for heterogeneous undocking kinetics? The difference in thermodynamic stability ($\Delta\Delta G_{dock}$) between the three less stably docked states and the most stable one (1.4, 2.7, and 3.7 kcal/mol, respectively) is consistent with the loss of one or a few hydrogen bonds (*30, 31*). Biochemical

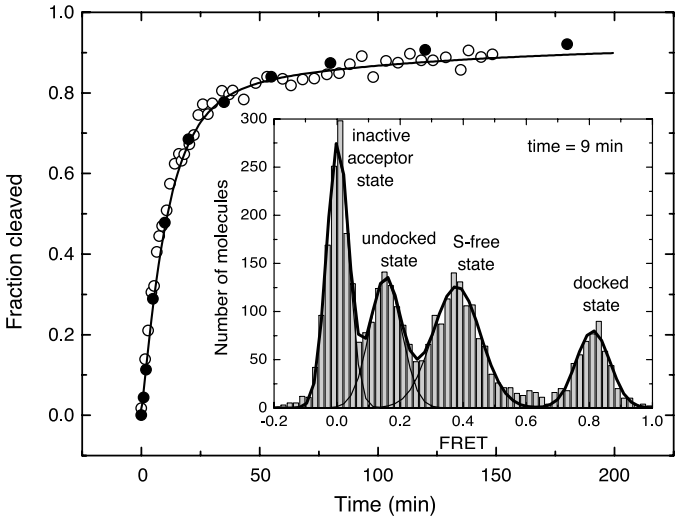

Fig. 2. Single-molecule and bulk solution measurements of enzymatic activities. The open symbols show the reaction time course of surface-immobilized ribozyme. For initiation of cleavage, a buffer containing 200 nM S was added to the immobilized ribozymes for 30 s to allow S binding; S was then removed from the buffer. During the reaction, the FRET distribution showed three distinct ribozyme populations: undocked (FRET ~0.15), docked (~0.81), and S-free ribozymes (~0.38). The peak at FRET ~0 was due to inactive Cy5 (*7*). The S-free fraction is plotted against time. In a control experiment with noncleavable S [with a 2′-O-methyl modification at the cleavage site, S(2′OMeA-1)], the S-free fraction accumulated with a rate constant slower than $4 \times 10^{-5}\ s^{-1}$, indicating that S dissociation is much slower than cleavage. The solid symbols show the reaction time course for the same ribozyme free in solution, as determined by gel electrophoresis and autoradiography (*21*). The data cannot be fit by a single-exponential function, indicating heterogeneous reaction kinetics. The solid curve is a numerical fit using the rate equations given in (*25*).

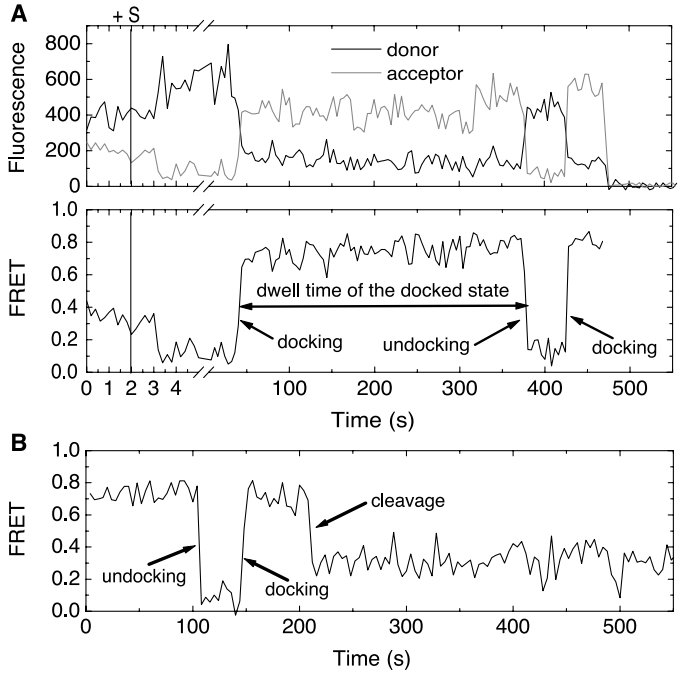

Fig. 3. Following the structural dynamics and function of single ribozyme molecules. (**A**) Typical fluorescence time trace of a single ribozyme upon S binding. Standard buffer containing 200 nM S(2′OMeA-1) was added to the sample at 2 s. The delay between S arrival and FRET signal change is consistent with the binding rate of S. Fluorescence signals from the donor and acceptor are indicated by solid and gray lines, respectively. (**B**) FRET time trace of a single ribozyme-cleavable S complex, showing docking, undocking, and cleavage as indicated.

and x-ray crystallography experiments show that loops A and B make several structurally important tertiary hydrogen bonds in the docked state (Fig. 1A) (*14, 18, 32*). It is plausible that different subsets of these hydrogen bonds are formed in the four distinct docked states observed here.

To test this hypothesis, we performed two mutation experiments: (i) In the g+1a mutant, all three hydrogen bonds in the g+1-C25 base pair (Fig. 1A) are disrupted and no docking is observed. (ii) In the g+1a/C25U mutant, two undocking rate constants (0.17 s^{-1} and 6 s^{-1}) are observed. (The docking rate constant is essentially unchanged, with $k_{dock} = 0.007\ s^{-1}$.) Comparing the most stably docked state of this mutant with that of the SV5 EH4 ribozyme, the energetic penalty for changing the g+1-C25 to the weaker a+1-U25 Watson-Crick base pair is $\Delta\Delta G_{dock} = 2.0$ kcal/mol, supporting the notion that the less stably docked states may be caused by disruption of interloop hydrogen bonds.

We have also measured the docking and undocking kinetics of the ribozyme in complex with cleavage products. In the presence of 17 μM 3′P and 17 μM 5′P [concentrations much higher than the equilibrium dissociation constants (*25*)], the ribozyme shows docking and undocking behavior similar to that seen with bound substrate. Docking can be described by a single rate constant, $k_{dock}^{3P5P} = 0.02\ s^{-1}$. Undocking shows heterogeneous kinetics with four rate constants: $k_{undock,1}^{3P5P} = 0.008\ s^{-1}$, $k_{undock,2}^{3P5P} = 0.04\ s^{-1}$, $k_{undock,3}^{3P5P} = 0.3\ s^{-1}$, and $k_{undock,4}^{3P5P} = 3\ s^{-1}$, with $k_{undock,1}^{3P5P}$ being predominant and also with a pronounced memory effect. The undocking rate constants did not change when the concentrations of 3′P and 5′P were decreased to a subsaturating 0.2 μM. At this concentration, once 5′P dissociates, the ribozyme will undock long before another 5′P binds to the ribozyme [$k_{undock}^{3P} = 64\ s^{-1}$ for ribozyme with bound 3′P (*25*)]. Thus, 5′P must be bound to the ribozyme throughout the time that the molecule resides in the docked state, except for perhaps the last few ms. The same consideration is true for 3′P. Once in the undocked state, product release is fast relative to docking (*25*). Thus, the effective rate constants for product release after cleavage are approximately equal to the observed undocking rate constants.

Because product release is predominantly slow (0.008 s^{-1}) compared to ligation [$k_{lig} \geq 0.2\ s^{-1}$ (*25*)], bond scission and ligation reach equilibrium long before the products are released. The overall cleavage reaction rate is thus not limited by bond-scission chemistry but by the slow docking and undocking transition and the internal equilibrium between cleavage and ligation. This explains its shallow pH dependence (*20*).

We now show that the combination of multiple undocking rates and the memory effect result in the overall heterogeneous cleavage reaction kinetics (*21, 22*). Qualitatively, when the enzyme-substrate complex docks into a stably docked state such that the reversible cleavage reaction reaches equilibrium long before undocking ($k_{undock} \ll k_{cleav} + k_{lig}$), the equilibrium constant k_{cleav}/k_{lig} determines the average number of docking-undocking cycles needed to release products and complete the reaction. By contrast, when the complex docks into an unstably docked state such that the cleavage reaction does not reach equilibrium before undocking ($k_{undock} > k_{cleav} + k_{lig}$), many more docking cycles are needed to release product, leading to a slower overall cleavage rate constant.

Quantitatively, we have used a set of rate equations to describe the kinetic reaction scheme shown in Fig. 1B. We assume perfect "memory" of the undocking rates, with substrate and product undocking rates correlated pairwise such that 61% of the population undock with rate constants $k_{undock,1} = 0.005\ s^{-1}$ and $k_{undock,1}^{3P5P} = 0.008\ s^{-1}$, 9% undock with

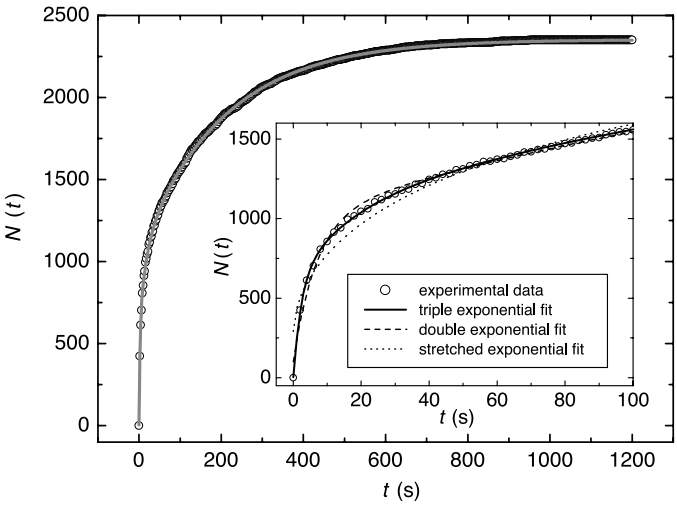

Fig. 4. The undocking kinetics is complex, suggesting four docked states of distinct stabilities. Plotted are the number of events (*N*) with dwell times of the docked state shorter than *t*. The dwell times were determined from time trajectories similar to those shown in Figs. 3 and 5. Two separate experiments—experiment A, with a lower time resolution (2 s) and photobleaching rate (0.001 s^{-1}), and experiment B, with a higher time resolution (0.1 s) at the expense of a higher photobleaching rate (~0.02 s^{-1})—were carried out. Dwell times of the docked state from experiment A are shown. The line is a triple-exponential fit that gives three rate constants for undocking: $k_{undock,1} = 0.005\ s^{-1}$, $k_{undock,2} = 0.06\ s^{-1}$, and $k_{undock,3} = 0.5\ s^{-1}$. The inset shows the comparison of the triple, double, and stretched exponential fits. The large discrepancy between the latter and the data shows that the process is better described by a number of discrete rate constants rather than a Gaussian distribution of rate constants. [Plots of the dwell times of the undocked state from experiment A and the dwell times of the docked state from experiment B are given in (*25*).] A triple-exponential fit of experiment B yields $k_{undock,2} = 0.06\ s^{-1}$, $k_{undock,3} = 0.5\ s^{-1}$, and $k_{undock,4} = 3\ s^{-1}$. The first two rate constants agree with the last two in experiment A, further supporting the notion of multiple discrete rate constants. The slowest rate constant, $k_{undock,1}$, does not appear in experiment B because of the fast photobleaching; $k_{undock,4}$ does not appear in experiment A because of the low time resolution. The fractions of time that the molecules undock with the four rate constants are 61%, 9%, 16%, and 14%, respectively.

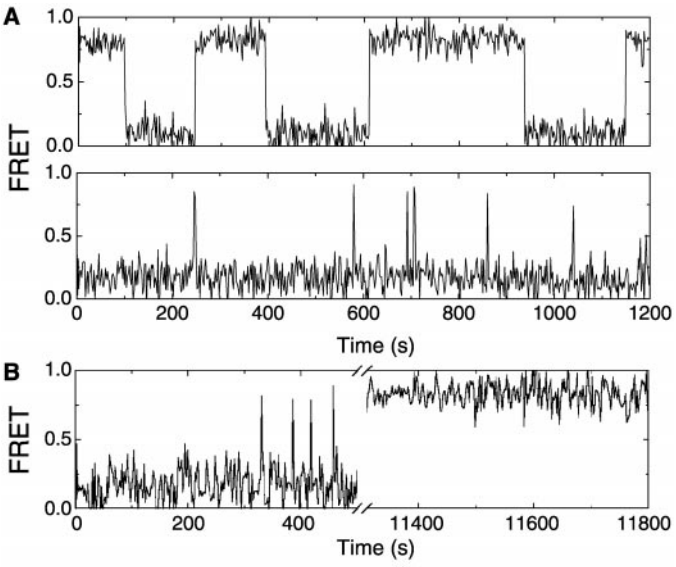

Fig. 5. Docked states have a strong memory effect, as indicated by FRET time traces of single ribozyme–S(2′OMeA-1) complexes. (**A**) Memory effect of the undocking kinetics where a molecule rarely switches between different docked states. (**B**) An example of memory loss after 3 hours. The excitation was shut off after ~500 s for 3 hours to prevent dye photobleaching.

$k_{undock,2} = 0.06\ s^{-1}$ and $k^{3P5P}_{undock,2} = 0.04\ s^{-1}$, etc. (see Fig. 4). The numerical solution of this set of coupled differential equations is plotted in Fig. 2. The fitted solution uses $k_{cleav} = 0.12\ s^{-1}$, $k_{lig} = 0.24\ s^{-1}$, and the fact that 7% of the enzymes are not active. The fit determines the equilibrium constant $k_{cleav}/k_{lig} = 0.5$ to better than ±30% and places an upper limit on $k_{lig} \leq 0.8\ s^{-1}$. [See (*25*) for a full description of this numerical work.]

Finally, we propose a model for the memory effect based on slow transitions between different structural configurations of loops A and B. The structures of these loops in the undocked state determined by NMR (*16, 17*) are different from those in the docked state determined by x-ray crystallography (*18*). We propose that loops A and B can adopt different conformations in the undocked state. If each loop has two possible conformations that favor a deeply docked and a loosely docked state, respectively, then their four combinations lead to four undocking rates, as are observed. The slow transition time between these loop conformations determines the memory time of the undocking rates. If only one of the two loops undergoes such transitions, it would require four different metastable conformations of this loop to give the four undocking rates.

Indeed, both NMR studies of loops A and B have given evidence of metastable alternating conformations, such as sharp resonance peaks for protonated and unprotonated species of A10 in loop A (*16*) and weak resonances detected between bases in loop B (*17*), but well-defined alternate structures were not proposed. Future research should test this hypothesis with a series of mutations that alter the structures of loops A and B to favor certain docked states at the expense of others.

Our single-molecule results demonstrate a tight coupling of structural dynamics and catalytic function in the hairpin ribozyme. Strikingly, the hairpin ribozyme—one of the simplest RNA enzymes—shows very complex structural dynamics, with four docked states of distinct stabilities and a strong memory effect. Our observations would be difficult to obtain by ensemble methods because the less stable conformational states are nonaccumulative. This work highlights the power of single-molecule approaches in characterizing complex structural dynamics.

References and Notes

1. R. F. Gesteland, T. R. Cech, J. F. Atkins, *The RNA World* (Cold Spring Harbor Laboratory Press, Cold Spring Harbor, NY, ed. 2, 1999).
2. H. F. Noller, *Annu. Rev. Biochem.* **60**, 191 (1991).
3. P. Nissen, J. Hansen, N. Ban, P. B. Moore, T. A. Steitz, *Science* **289**, 920 (2000).
4. C. A. Collins, C. Guthrie, *Nature Struct. Biol.* **7**, 850 (2000).
5. S. Valadkhan, J. L. Manley, *Nature* **413**, 701 (2001).
6. E. A. Doherty, J. A. Doudna, *Annu. Rev. Biochem.* **69**, 597 (2000).
7. X. Zhuang *et al.*, *Science* **288**, 2048 (2000).
8. G. J. Schutz, W. Trabesinger, T. Schmidt, *Biophys. J.* **74**, 2223 (1998).
9. T. Ha *et al.*, *Proc. Natl. Acad. Sci. U.S.A.* **96**, 893 (1999).
10. T. Ha *et al.*, *Proc. Natl. Acad. Sci. U.S.A.* **96**, 9077 (1999).
11. N. G. Walter, J. M. Burke, *Curr. Opin. Chem. Biol.* **2**, 24 (1998).
12. N. G. Walter, K. J. Hampel, K. M. Brown, J. M. Burke, *EMBO J.* **17**, 2378 (1998).
13. N. G. Walter, J. M. Burke, D. P. Millar, *Nature Struct. Biol.* **6**, 544 (1999).
14. D. J. Earnshaw *et al.*, *J. Mol. Biol.* **274**, 197 (1997).
15. R. Pinard *et al.*, *J. Mol. Biol.* **307**, 51 (2001).
16. Z. Cai, I. Tinoco, *Biochemistry* **35**, 6026 (1996).
17. S. E. Butcher, F. H. Allain, J. Feigon, *Nature Struct. Biol.* **6**, 212 (1999).
18. P. B. Rupert, A. R. Ferre-D'Amare, *Nature* **410**, 780 (2001).
19. S. M. Nesbitt, H. A. Elacher, M. J. Fedor, *J. Mol. Biol.* **286**, 1009 (1999).
20. M. J. Fedor, *J. Mol. Biol.* **297**, 269 (2000).
21. J. A. Esteban, A. R. Banerjee, J. M. Burke, *J. Biol. Chem.* **273**, 13629 (1997).
22. J. A. Esteban, N. G. Walter, G. Kotzorek, J. E. Heckman, J. M. Burke, *Proc. Natl. Acad. Sci. U.S.A.* **95**, 6091 (1998).
23. The hairpin sequence we used is based on the optimized SV5 EH4 hairpin ribozyme (*12*). The 2′OMeA-1 substrate was used when measuring the docking and undocking rates independent of cleavage. Cy5-labeled RzA and biotin-labeled RzB were synthesized by the RNA synthesis facility of the University of Vermont. Cy3 was coupled to the 3′ end of RzA postsynthetically, via a primary amine attached to the 3′-most phosphate. All single-stranded RNAs used in the experiment were purified by gel electrophoresis and C_8 reversed-phase high-performance liquid chromatography as described (*12*) to >95% purity. To form the ribozyme, we annealed RzA to RzB by heating to 80°C for 1 min and then slowly cooling to 22°C in 50 mM tris-HCl (pH 7.5) and 12 mM $MgCl_2$. These standard buffer conditions were used in all experiments. In single-molecule experiments, an oxygen scavenger system (*7*) was added to the buffer to show photobleaching.
24. The distance between the 3′ and 5′ ends of RzA in the docked state was estimated using a recent crystal structure (*18*). The distance in the undocked state was estimated under the assumption that the structures of the two domains are similar to those in the docked state but are coaxially stacked. The distance in the S-free state was estimated under the assumptions that domain B has a similar structure as in the docked state, whereas the single-stranded overhang is a random coil with complete flexibility between adjacent nucleotides. These distances compare very well with a previous measurement by time-resolved FRET (*13*).
25. Methods are available as supporting material on *Science* Online.
26. H. P. Lu, L. Xun, X. S. Xie, *Science* **282**, 1877 (1998).
27. L. Edman, R. Rigler, *Proc. Natl. Acad. Sci. U.S.A.* **97**, 8266 (2000).
28. J. D. Rabinowitz *et al.*, *Immunity* **9**, 699 (1998).
29. E. Z. Eisenmesser, D. A. Bosco, M. Akke, D. Kern, *Science* **295**, 1520 (2002).
30. J. SantaLucia, R. Kierzek, D. H. Turner, *Science* **256**, 217 (1992).
31. S. K. Silverman, T. R. Cech, *Biochemistry* **38**, 8691 (1999).
32. R. Pinard *et al.*, *EMBO J.* **20**, 6434 (2001).

33. We thank E. Sarajlic, S. Blanchard, R. Gonzales, M. Fedor, and D. Herschlag for helpful suggestions. Supported in part by an NSF grant (S.C.) and NIH grant GM62357 (N.G.W.), an NIH postdoctoral fellowship and Harvard University (X.Z.), a Center on Polymer Interfaces and Macromolecular Assemblies NSF grant (H.P.B.), and a Stanford graduate fellowship (H.K.).

Supporting Online Material
www.sciencemag.org/cgi/content/full/296/5572/1473/DC1
Methods
Figs. S1 to S5
References

14 December 2001; accepted 19 April 2002

Functional Neuroanatomical Differences Between Adults and School-Age Children in the Processing of Single Words

Bradley L. Schlaggar,[1,5]* Timothy T. Brown,[3] Heather M. Lugar,[1] Kristina M. Visscher,[4] Francis M. Miezin,[1,2] Steven E. Petersen,[1,2,3,4]

A critical issue in developmental cognitive neuroscience is the extent to which the functional neuroanatomy underlying task performance differs in adults and children. Direct comparisons of brain activation in the left frontal and extrastriate cortex were made in adults and children (aged 7 to 10 years) performing single-word processing tasks with visual presentation; differences were found in circumscribed frontal and extrastriate regions. Conceivably, these differences could be attributable exclusively to performance discrepancies; alternatively, maturational differences in functional neuroanatomy could exist despite similar performance. Some of the brain regions examined showed differences attributable to age independent of performance, suggesting that maturation of the pattern of regional activations for these tasks is incomplete at age 10.

A fundamental objective in basic and clinical neuroscience is to understand the development of the functional organization of the human brain. Such knowledge can not only illuminate normal functional anatomical development (*1*) but also create a context for understanding the consequences of early perturbations to the developing brain (*2*, *3*) or